Chapter 3

Calorimetry in High-Energy physics

The name calorimeters refers to the detectors that measure the energy and position of the particles by means of their total absorption or destruction in such detectors. The absorption process always takes place through the secondary particle generation that interact as well with the detector in their sine.

Conceptually, a calorimeter consists of a matter block that serves to intercept primary particles, and has sufficient thickness so that all the energy of the radiation, originated by the primary particle and the created ones in the subsequent cascade, is deposited in its interior. The energy of a particle is degraded to the level of detectable atomic ionizations and excitations. Calorimeters are used to measure not only the energy, but also the spatial position, the direction and, in some cases, the nature of the primary particle. Some fraction of the deposited energy could be detected as a usefull signal (e.g. scintillation light, Cherenkov light or ionization charge), which should be proportional to the initial energy.

Calorimeters offer many atractive capabilities, supplementing or replacing the information obtained with magnetic spectrometers:

- They are sensitive to charged and neutral particles.

- The energy degradation through the development of the particle shower is a statistical process, and the average number $\langle N \rangle$ of secondary particles is proportional to the energy of the incident particle.

- The length of the detector increases logarithmically with the particle energy E.

- With segmented detectors, the information on the shower development allows precise measurements of the incident particle coordinates.

• The different response to electrons, muons and hadrons can be exploited for particle identification.

• Their fast time response allows the operation with high particle rates, and the pattern of the energy deposition can be used for fast on-line event selection.

According to the detected type of particle and the generated cascades, the calorimeters are classified:

• *Electromagnetic calorimeters.* The photons and the electrons interact electromagnetically with the absorber material through the following processes:

i) bremsstrahlung

ii) pair production

iii) Compton scattering

iv) photo-electric effect.

The cross-section of these processes and the multiplicity of the particles that take place in the cascade determine the characteristics of these instruments. The typical electromagnetic calorimeters scale is about 10 times the radiation length X_0.

• *Hadronic calorimeters.* The hadrons interact strongly with the absorber material. The absorption length λ of hadrons in the material is the appropriate scale to have an idea of its size ($\lambda >> X_0$).

In this chapter we comment on the main features of electromagnetic showers (section 3.1) and hadronic showers (section 3.2). In section 3.3 we will discuss how the e/h ratio affects the calorimeter performance. Section 3.4 is devoted to the description of the principle and physics requirements of the Tile Calorimeter as one of the sub-detectors of the ATLAS spectrometer.

3.1 Electromagnetic showers

The electromagnetic interaction can be manifested through:

a) Scintillation light produced by de-excitations of atoms and molecules excited by charged radiation,

b) Cherenkov light originated by electrons when the medium has a refraction index $n > 1$,

c) bremsstrahlung radiation, with photon emission and the subsequent pair production (basic processes in the electromagnetic showers development),

d) nuclear reactions with fragmentation of the target nucleus and production of secondary hadrons with a very low cross-section.

The behaviour of photons in matter is different from that of charged particles, the main interactions which can undergo are:

- Photo-electric effect.
- Compton scattering.
- Pair production.

The contribution of the various energy loss mechanisms as a function of the particle energy are given in figure 3.1, for electrons and positrons, and in figure 3.2 for photons [1]. Above approximately 1 GeV the principal processes (bremsstrahlung for electrons and positrons, and pair production for photons) become energy independent. It is through a succession of these energy loss mechanisms that the electromagnetic cascade (EMC) is propagated, until the energy of the charged secondaries has been degraded to the regime dominated by ionization loss. Within this description, the combined energy loss of the cascade particles in the detector equals the energy of the incident electron or photon.

The measurable signal (excitation or ionization of the medium) can be considered as the sum of the signals from the track segments of the positrons and electrons. The quantity which is usually introduced to represent the spatial development of the shower is the differential distribution of the *track length* T, defined as the sum of the tracks of all the charged particles in the shower.

The electromagnetic shower is fully described by quantum electrodynamics (QED)[2], and depends essentially on the density of electrons in the absorber medium. For this reason it is possible to describe the characteristic longitudinal dimensions of the high-energy EMC (E > 1 GeV) in a material-independent way, using the *radiation length* X_0. The energy loss ΔE due only to radiation in a distance Δx can then be written as:

$$(\Delta E)_{radiation} = -E(\Delta x/X_0) \tag{3.1}$$

and the X_0 numerical value is well approximated by the following expression:

$$X_0\ [g/cm^2] \sim 180A/Z^2\ (to\ better\ than\ 20\%\ for\ \sim\ Z > 13). \tag{3.2}$$

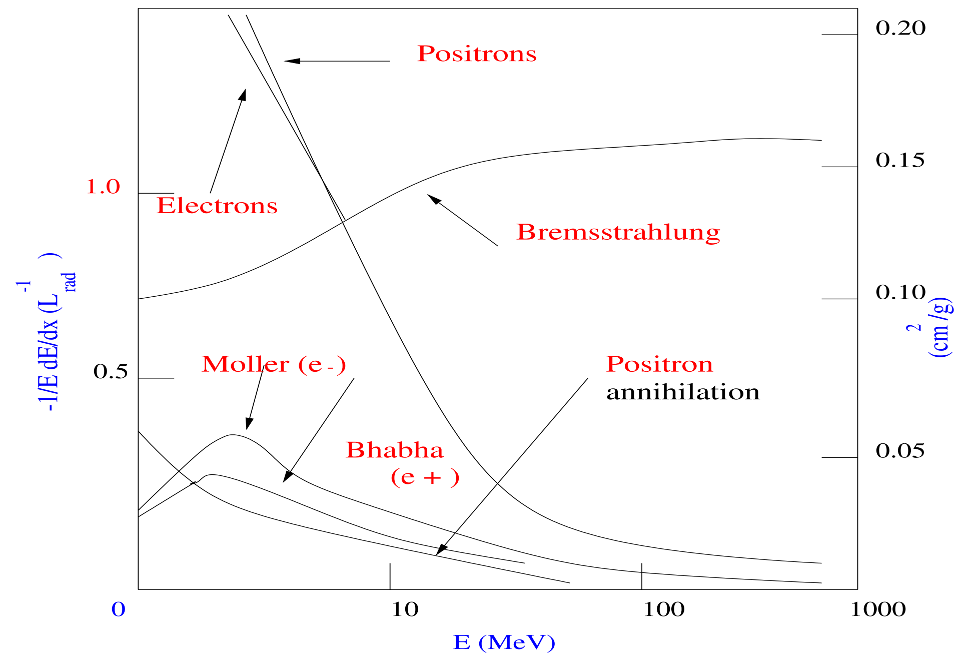

Figure 3.1: Fractional energy loss per radiation length (left ordinate) and per g/cm^2 (right ordinate) in lead as a function of electron or positron energy.

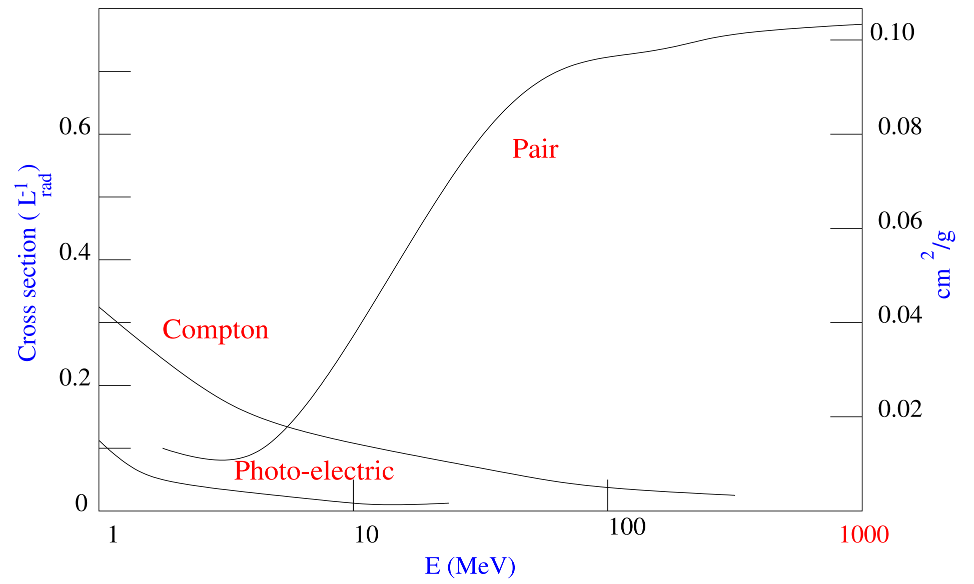

Figure 3.2: Photon cross-section σ in lead as a function of the photon energy. The intensity of photons can be expressed as $I = I_0 exp(-\sigma x)$, where x is the path distance in radiation length units.

Whilst the high-energy part of the EMC is governed by the value of X_0, the low-energy tail of the shower is characterized by the *critical energy* ϵ of the medium. It is defined as the energy loss by *collisions* of electrons or positrons of energy ϵ in the medium in one radiation length, i.e:

$$(dE)_{collision} = -\epsilon(dx/X_0) \tag{3.3}$$

where ϵ (MeV) is approximately $550 \times Z^{-1}$ (accurate to better than 10% for $Z > 13$). This value of ϵ coincides with the value of the electron energy below which the ionization energy loss starts to dominate the energy loss by bremsstrahlung.

The characteristic longitudinal EMC profile is shown in figure 3.3, for four very different materials, and demonstrates the *longitudinal scaling in radiation length.* A convenient analytical description of the profiles has been given in the form [3]:

$$dE/dt = E_0 b^{\alpha+1}/\Gamma(\alpha+1)t^{\alpha}e^{-bt} \tag{3.4}$$

where $t = x/X_0$, $\alpha = bt_{max}$ and $b \sim 0.5$.

The transverse shower properties can also be easily understood qualitatively. At the beginning, where is the most energetic part of the cascade, the lateral spread is characterized by both the typical angle for bremsstrahlung, $\theta_{brems} \sim p_e/m_e$, and the multiple scattering in the absorber. This latter process produces an increasment of the lateral spread when the energy of the shower particles decreases and consequently causes a gradual widening of the shower. For the purpose of total energy measurement, the EMC occupies a cylinder of radius R:

$$R \approx 2\rho_M; \qquad \rho_M = 21X_0/\epsilon \approx 7A/Z \; [g \; cm^{-2}], \tag{3.5}$$

ρ_M being the *Molière Radius*, which describes the average lateral deflection of electrons of energy ϵ after traversing one radiation length.

3.1.1 Rossi-Heitler model

This is a simple but useful model of the development of the electromagnetic shower from the energetic point of vue.

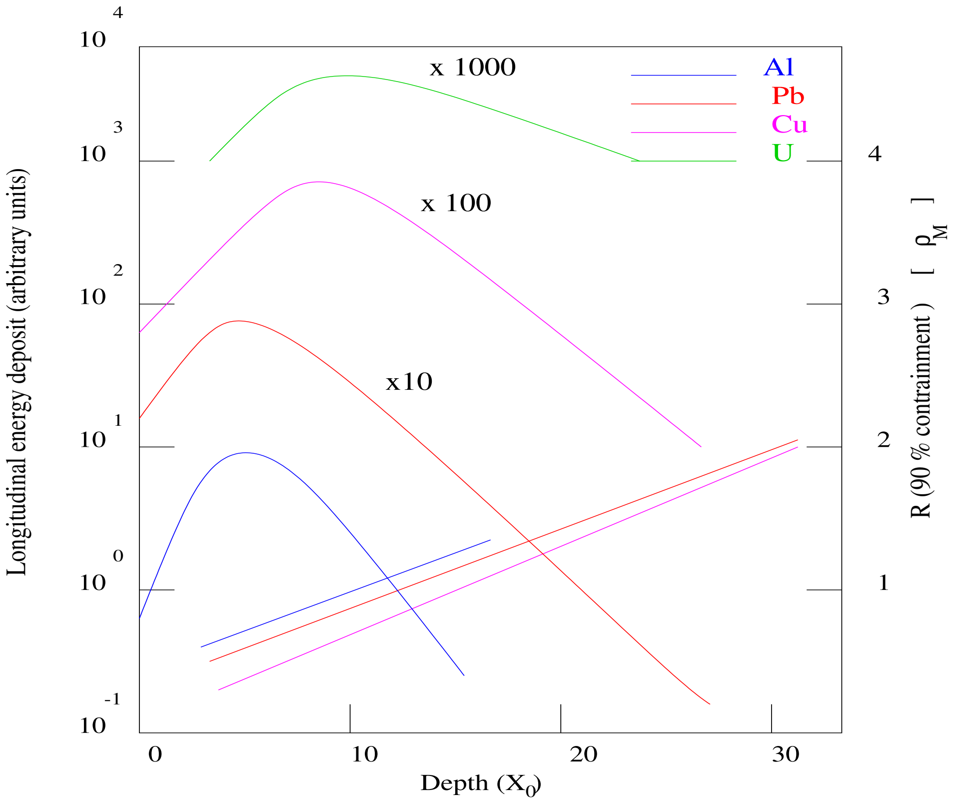

Figure 3.3: Longitudinal shower development (left ordinate) of 6 GeV/c electrons in four very different materials, showing the scaling in units of radiation length X_0. On the right ordinate the shower radius for 90% containment of the shower is given as a function of the shower depth. In the later development of the cascade, the radial shower dimensions scale with the Molière radius $\rho_M \sim 7A/Z$.

The development of the electromagnetic cascade can be parametrized in a simple form, if we follow the hypotheses of Rossi:

• After crossing a radiation length X_0, the electrons radiate by bremsstrahlung a photon, being the photon and electron energies: $E_\gamma = E_{in}/2 = E_e$.

• Moreover, after crossing a radiation length X_0 the energetic photons should be materialized in a pair e^+ e^- with symmetrical distribution of energy: $E_{e^+} = E_\gamma/2 = E_{e^-}$.

• The Compton effect and the electron energy loss by ionization or excitation are not considered for $E_e > \epsilon$, being ϵ the critical energy.

• The shower development stops when $E_e = \epsilon$.

The simple image of the model can be observed in the figure 3.4.

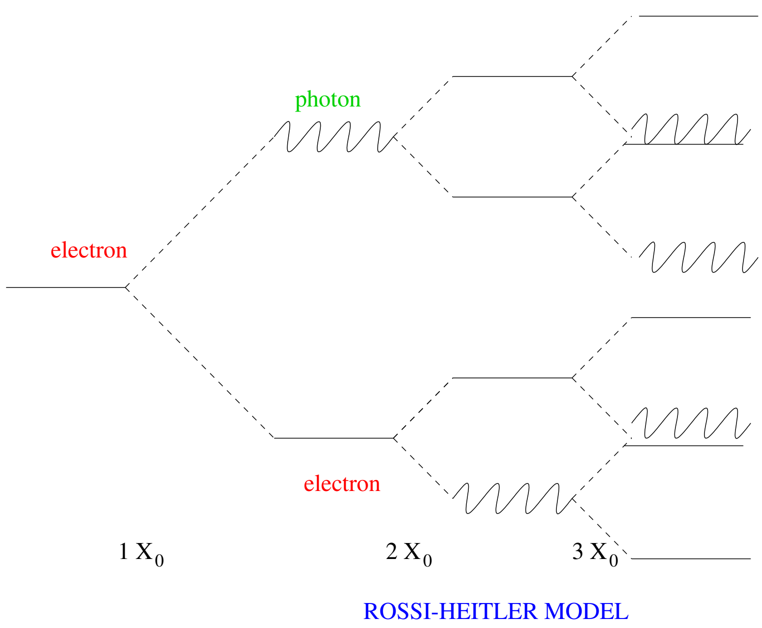

Figure 3.4: Schematic representation of the development of an electromagnetic shower according to the Rossi-Heitler model. X_0 is the radiation length.

An inmediate conclusion of the model is that after t radiation lengths, the number of particles that will be in the shower is:

$$N = 2^t \tag{3.6}$$

and the energy of each particle will be:

$$E = E_{in}/2^t. \tag{3.7}$$

The number of particles with an energy greater than E is growing exponentially with t, from $t = 0$ to $t = t_{max}$, where:

$$t_{max} = \frac{ln(E_0/\epsilon)}{ln2} \tag{3.8}$$

$$N_{max} = E_0/\epsilon$$

Although the Rossi model is quite simple it can reproduce interesting properties of electromagnetic showers:

- Concept of the maximum development of the shower, t_{max}.
- Linearity between E_{in} and the number of particles generated in the shower.
- Logarithmic growth of the longitudinal development of the shower with the incident energy E_{in}.

The number of particles with energy greater than a prefixed value E' can be calculated like:

$$N(E > E') = \int_0^{t(E')} N(t)dt \sim \frac{1}{ln2}\frac{E_0}{E'}, \tag{3.9}$$

where $N(t) = 2^t$; for this reason the energetic espectrum of the shower decreases like $1/E^2$.

In the same way, the total length of charged tracks in the shower is proportional to the incidente energy:

$$L = \frac{2}{3}\int_0^{t_{max}} N(t)dt \sim \frac{E_0}{\epsilon}. \tag{3.10}$$

The 2/3 factor is the fraction of charged tracks.

3.1.2 Classification of the electromagnetic calorimeters

Conceptually there exist two types of different detectors for the identification and measurement of the energy and position of the $e^{\pm}$, γ based on the formation of the electromagnetic showers:

• *Homogeneous calorimeters*: These calorimeters combine in a single material the active and passive functions. The medium acts at the same time as the absorber in which the multiplication of the secondary particles takes place and therefore the shower development (passive function), and is where the energy deposited by the secondary particles is converted in a detectable signal (active function).

Some examples of these calorimeters are the INa(Tl), BGO crystals and the lead glass counters.

• *Heterogeneous calorimeters*: For these detectors the materials for the active and passive functions are different. The method allows the optimal selection of both materials (high Z for the absorber and low Z for the active medium).

Traditionally these detectors are constituted by an alternate succession of absorber (generally Pb) and active material layers (scintillator, liquid argon, etc.).

3.1.3 Limits on Energy Resolution for Electromagnetic Calorimeters

The resolution of the measured energy is determined by the fluctuations in the shower propagation. The intrinsic component of the resolution is caused by the fluctuations in T_d (the *detectable* track length). This represents the lower bound on the energy resolution. In practical detectors, usually a number of additional components must be considered, which may affect the resolution. One important instrumental contribution to the energy resolution comes from the incomplete containment of the showers (*energy leakage*). The longitudinal containment of the shower can be parametrized, on average, as:

$$L(98\%)_{av} \approx t_{max} + 4\lambda_{att} \tag{3.11}$$

where $L(98\%)$ gives the length for the 98% longitudinal containment. The quantity λ_{att} characterizes the slow exponential decay of the shower after the shower maximum (see figure 3.3). The values of λ_{att} are found to be rather energy independent, but material dependent and close in value to the mean free path of photons that have minimum attenuation in a given material. The effect of the longitudinal leakage on the energy resolution is consistent with the parametrization:

$$\sigma(E)/E \approx [\sigma(E)/E]_{f=0} \times [1 + 2\sqrt{E(GeV)} \times f] \tag{3.12}$$

being f the fractional energy loss through leakage. For values of $f < 0.2$ and $E < 100\ GeV$, one notes that the longitudinal leakage is more critical than the transverse leakage due to the fact that the fluctuations around the average longitudinal loss are much larger than for transverse leakage.

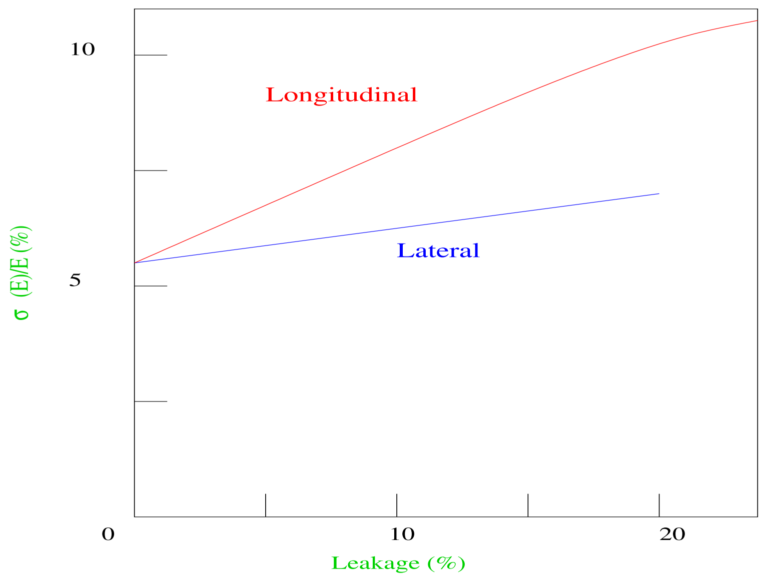

Figure 3.5: Effects of longitudinal and lateral losses on the energy resolution as measured for electrons in the CHARM neutrino calorimeter [4].

3.1.4 Energy resolution in “Sampling” calorimeters

Sampling calorimeters are devices in which the functions of energy degradation and energy measurement are separated in alternating layers of different substances. The choice of a *pasive* absorber (typically plates made of Fe, Cu, or Pb, each ranging in thickness from a fraction of X_0 to a few X_0) makes possible to build rather compact devices and permits optimization for a specific experimental requirement such as electron/pion discrimination or position measurement. The disadvantage is that only a fraction of the total shower energy is *sampled* in the active planes, resulting in additional fluctuations of the energy determination. Today we know that the energy resolution depends on the characteristics of both the passive and active medium (in particular, thickness and density) and because that several effects contribute to the *total* sampling fluctuations.

The *intrinsic sampling* fluctuations express the statistical fluctuations in the number of e^+e^- pairs traversing the active signal planes. The number N_x of crossings is:

$$N_x = T \ (total\ track\ length)/d \ (distance\ between\ active\ plates) \tag{3.13}$$

where $T = E/\epsilon$ and hence $N_x = E/\epsilon d = E/\Delta E$, ΔE being the energy loss per unit cell. The contribution to the energy resolution is:

$$\sigma(E)/E_{sampling} = \sigma(N_x)/N_x = 1/\sqrt{N_x} = 3.2\% \ [\Delta E \ (MeV)/E \ (GeV)]^{1/2} \tag{3.14}$$

This expression has to be regarded as a lower bound on the sampling fluctuations, due to the following reasons:

• tracks originate from pair-produced particles and therefore the number of independent gap crossings would be only $N_x/2$ for totally correlated production;

• it ignores multiple scattering, which increases the effective distance d to $d = d \,/\, \langle \cos\theta \rangle$, where the characteristic multiple scattering angle θ is given by 21 $(MeV)/\epsilon\pi$ [5].

The energy resolution seems to be rather well described by these estimates, provided that instrumental effects (such as calibration errors, photon statistics, leakage, etc.) do not dominate.

3.2 Hadronic showers

Hadronic calorimeters are detectors whose objective is to measure the energy of the particles that are not completely absorbed in the electromagnetic calorimeters and therefore are normally located behind those electromagnetic devices. Usually the electromagnetic calorimeters suppose up to a few interaction lengths λ of the hadronic calorimeter, and consequently the first part of the hadronic shower is gathered in the electromagnetic calorimeter, this is the reason why the studies of combined calorimetry are becoming more and more popular.

The development of the hadronic shower in matter is so complicated that simplified analytical treatments are not available. Conceptually, the energy measurement of hadronic showers is analogous to that of EMCs, but the much greater variety and complexity of the hadronic processes propagating the hadronic shower (HC) complicate the detailed understanding.

Typical of the hadronic interactions is the multiple particle production with transverse momentum $\langle p_t \rangle \cong 0.35$ GeV/c, for which about half of the available energy is consumed (the inelasticity $K \cong 0.5$). The remaining energy is carried by fast forward-going (leading) particles. The secondaries are mostly pions and nucleons, and their multiplicity is only weakly energy-dependent. The characteristic stages in the HC development are summarized in Table 3.1. Two specific features have been identified as the principal physical limitations to the energy resolution of hadronic calorimeters:

• A considerable part of the secondaries are π^0, which will propagate electromagnetically without any further nuclear interactions. The size of the π^0 component is largely determined by their production in the first interactions, and therefore, event-by-event fluctuations around the average value are important.

• A sizeable amount of the available energy is converted into excitation or break-up of the nuclei, of which only a fraction will result in detectable (*visible*) energy.

The two processes, intimately correlated, may lead for a given entering hadron, to a very different shower composition, which has a very different detectable response. They impose the intrinsic limitation on the performance of the hadronic calorimeters. Neutral pions amount is on average 1/3 of the produced pions and their energy is dissipated in the form of electromagnetic showers. The fraction of the total energy which is dissipated in ionizations by electrons and charged hadrons fluctuates from event to event and is the main contribution to the energy resolution in hadron calorimetry, because while the electromagnetic energy and the energy of the charged hadrons are well sampled, a large fraction of the remaining energy is not seen.

Table 3.1 gives some indications of the relative importance of these competing processes. Considerable knowledge has been gained from very detailed Monte Carlo calculations, which in their most ambitious form aim to simulate the full nuclear and particle physics aspects of the hadronic cascade based on the measured cross-section of the elementary processes [6]. Examples showing the energy dependence of the principal effects are given in figure 3.6. It should be noticed that these various processes contribute in varying degrees to the visible energy of the HC, and that a considerable fraction (such as nuclear binding energy, muons, and neutrinos) will be lost in the form of *invisible* or undetectable energy.

The longitudinal average and the transverse distributions are useful estimates of

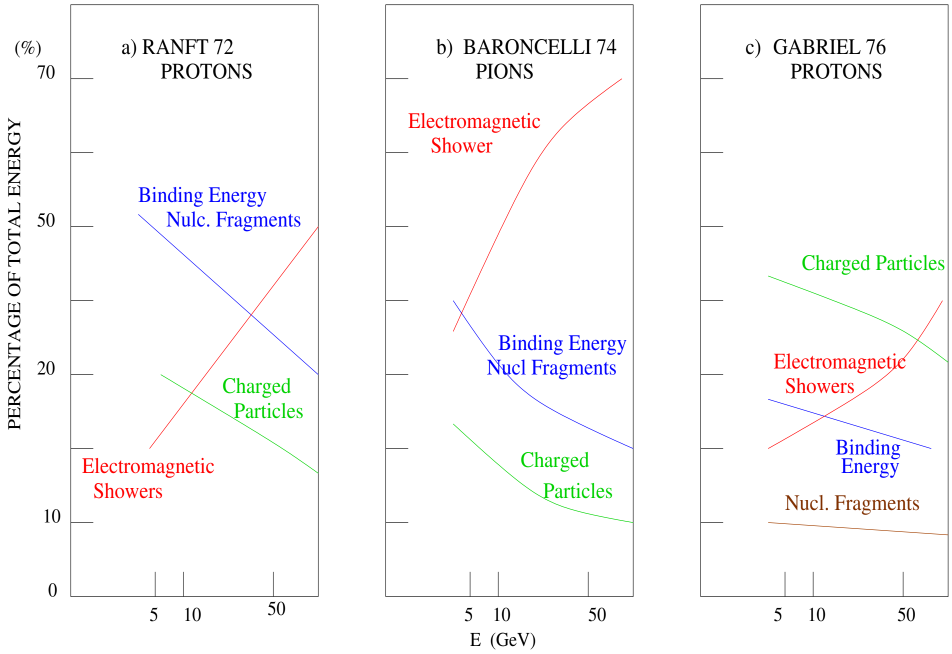

Figure 3.6: Relative contributions of the most important processes to the energy dissipated by hadronic showers in iron. The Monte Carlo calculations are by Ranft, Baroncelli and Gabriel [6].

Table 3.1: Properties of the phenomena which determine the development of hadronic showers.

Reaction	Properties	Influence on energy resolution	Charac. time (s)	Charac. length (g/cm^2)
Hadron production	Multiplicity $\cong A^{0.1}$ ln s Inelasticity $\cong 1/2$	π^0/π^+ ratio Binding energy loss	10^{-22}	Abs. length $\lambda \cong 35A^{1/3}$
Nuclear deexcitation	Evaporation energy $\cong 10\%$ Binding energy $\cong 10\%$ Fast neutrons $\cong 40\%$ Fast protons $\cong 40\%$	Binding energy loss Poor or different response to n, charged particles, and $\gamma's$	$10^{-18} - 10^{-13}$	Fast neutrons $\lambda_n \cong 100$ Fast protons $\lambda_p \cong 20$
Pion and muon decays	Fractional energy of $\mu's$ and $\nu's \cong 5\%$	Loss of $\nu's$	$10^{-8} - 10^{-6}$	$\gg \lambda$
Decay of c, b particles produced in multi- TeV cascades	Fractional energy of $\mu's$ and $\nu's$ at percent level	Loss of $\nu's$ Tails in resolution function	$10^{-12} - 10^{-10}$	$\ll \lambda$

the characteristic dimension for near-complete shower containment. The average longitudinal distribution exhibit *scaling in units of absorption length* λ. The transverse distribution depends (as in the case of EMCs) on the longitudinal depth: the core of the shower is rather narrow (FWHM from 0.1 to 0.5λ), increasing with the shower depth.

Experimental data are consistent with the following parametrization:

• The shower maximum, measured from the face of the calorimeter, is given by

$$t_{max}(\lambda) \sim 0.2 \; lnE \; (GeV) + 0.7 \tag{3.15}$$

and it occurs at a smaller depth in high-Z materials due to the smaller ratio of X_0/λ.

• The longitudinal dimension required for almost full containment is approximated by

$$L_{0.95}(\lambda) \cong t_{max} + 2.5\lambda_{att} \tag{3.16}$$

again measured from the face of the calorimeter. The quantity λ_{att} describes the exponential decay of the shower beyond t_{max} and increases with the energy approximately as $\lambda_{att} \cong \lambda\ [E\ (GeV)]^{0.13}$, with an indication of a weaker energy dependence for high-Z absorbers. The expression for $L_{0.95}$ describes the available data in the energy range from a few GeV to a few hundred GeV within 10%.

• The transverse radius R of the 95% containment cylinder is approximately $R_{0.95} \leq 1\ \lambda$; it does not scale with λ and is smaller in high-Z substances.

• A useful parametrization of the longitudinal shower development is

$$dE/ds = K[wt^a e^{-bt} + (1 - W)l^c e^{-dl}], \tag{3.17}$$

where $dE\ /\ ds$ is the longitudinal energy deposited, t is the depth, starting from the shower origin, in radiation lengths, and l is the same depth in units of absorption lengths. The parameters $a,\ b,\ c,\ d$ are obtained from a fit to the data and they show a logarithmic energy dependence.

3.2.1 Intrinsic energy resolution

The principal limitations to the hadron energy resolution are due to the fluctuations originated by the vastly different detection mechanisms for different particles (from π^0's to slow neutrons, muons, and neutrinos). These fluctuations have been found to be larger (of the order of 50% at 1 GeV) in strong contrast with the measurement of electromagnetic calorimeters, where the *intrinsic* fluctuations of the visible track length are less than 1% at 1 GeV. The dominant influence of the nuclear processes manifests itself also in the shape of the response function (figure 3.7) and is corroborated by detailed Monte Carlo estimates. Available experimental evidence indicates that the intrisic hadronic energy resolution is:

$$\frac{\sigma}{E} = \frac{45 - 50\%}{\sqrt{E}} \oplus b\%, \tag{3.18}$$

where the first term is atributed to shower fluctuations. It is sizeable because, about one fourth of the hadron energy E is not sampled and the fluctuations on the missing 25% are very large. The second term has the typical dependence of the energy resolution for electromagnetic showers, which is appoximately the fraction of the total energy dissipated in ionizations by electrons, positrons and charged hadrons.

The level of these nuclear effects and, more generally, the level of *invisible* energy is sensitively measured by comparing the calorimeter response for electrons and hadrons at the same *available* energy, which is the kinetic energy of electrons and nucleons, the total energy for mesons, and the total energy plus the rest mass for antinucleons.

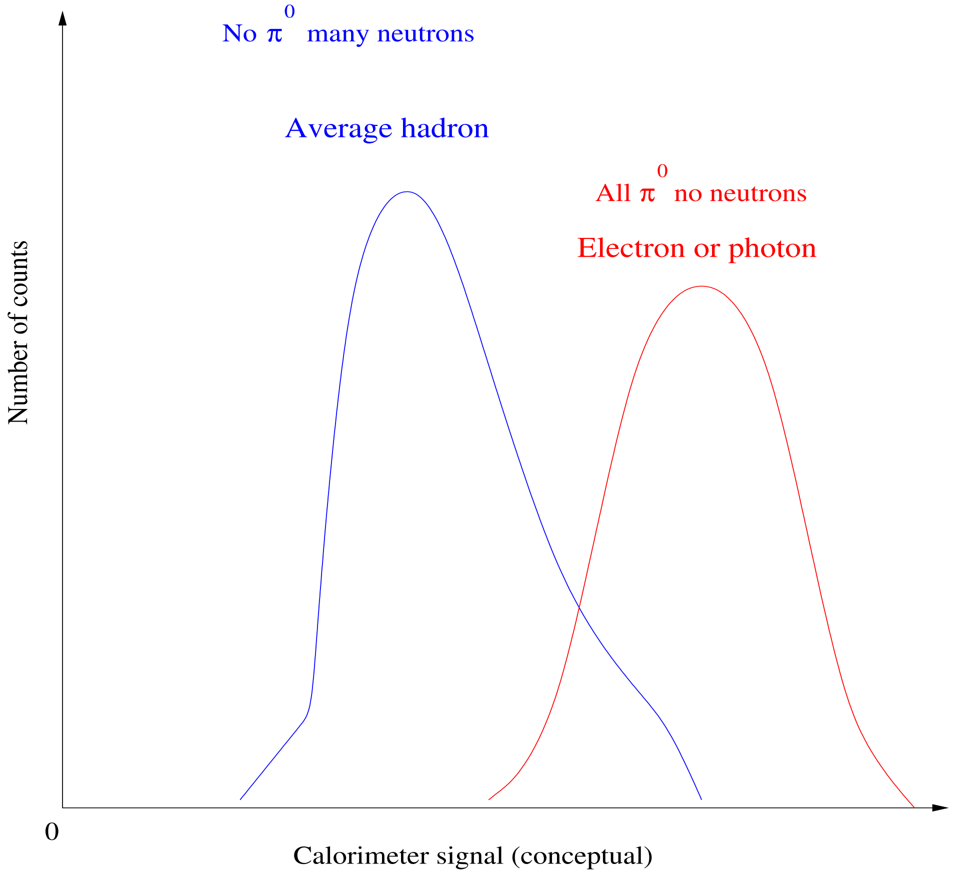

Figure 3.7: Calorimeter response for 10 GeV/c pions. The fluctuations are dominated by the nature of the first inelastic interaction. On average, a certain number of π^0's, charged pions, nuclear fragments, and slow protons and neutrons will be produced. At the other extreme the reaction products are mostly π^0's, and the energy deposit will be very similar to that of electrons or photons of equivalent energy.

All calorimeters except those made from uranium show a visible energy of approximately 70% relative to electrons (for uranium especially designed calorimeters, the nuclear losses are effectively compensated, leading to a response that is nearly equal for charged and neutral pions), which slowly increases owing to the rise in the electromagnetic component at higher energies. At low-energy limit all calorimeters, including those using uranium as a degrader, are expected to give similar responses. This interpretation is confirmed by the fact that in this limit the relative resolution improves.

In summary, the response of hadrons relative to electrons in a calorimeter is a sensitive probe of the level of nuclear effects. The intrinsic resolution of hadron calorimeters is limited to $\frac{\sigma}{E} = \frac{45-50\%}{\sqrt{E}} \oplus b\%$. The material and energy dependence of the limiting resolution is the most important open problem in hadron calorimetry.

3.2.2 Compensating fluctuations (Methods to reduce the effects of fluctuations)

We have emphasized that the relative response between electrons and pions is a sensitive measure of the level of nuclear interactions. An improvement in the energy resolution would be expected if the response of the electromagnetic cascade were identical compared with the purely hadronic one.

Several suggestions have been made for monitoring the level of the electromagnetic componet measured event-by-event. One suggestion was to use, as an indicator, the Cherenkov light from relativistic particles mainly produced by e^+e^- pairs [7], but Monte Carlo estimates for practical devices suggest that it is difficult to obtain a very useful correlation and to improve the resolution significantly. Another suggestion was to monitor the level of the nuclear component by associating heavily ionizing particles with the *late* component of the hadronic shower [8]. The most successful attempt was done by a weighting algorithm applied to the individual longitudinal measurements relative to the total energy measured. In figure 3.8 the unweighted and weighted results for the energy resolution are presented. Firstly, it can be seen that the raw results show a marked deviation from the expected $E^{-1/2}$ dependence. Secondly, the weighting algorithm improves the resolution, particularly at the highest energies, to a level that would be expected from extrapolating the low-energy resolution according to an $E^{-1/2}$ law.

The more direct cure for these fluctuations is the uranium hadronic calorimeter to compensate the fluctuations due to the missing energy with the nuclear fissions produced by neutrons in uranium. With an argon-uranium calorimeter of these characteristics the hadron resolution is $\sim 30\%\sqrt{E}$, definitely much better than the resolution obtained with iron calorimeters. The improved resolution goes together with an increase of the ratio between the visible energies for pions and electrons from $\pi/e \sim 0.70$ in argon-iron to $\pi/e \sim 1.05$ in argon-uranium.

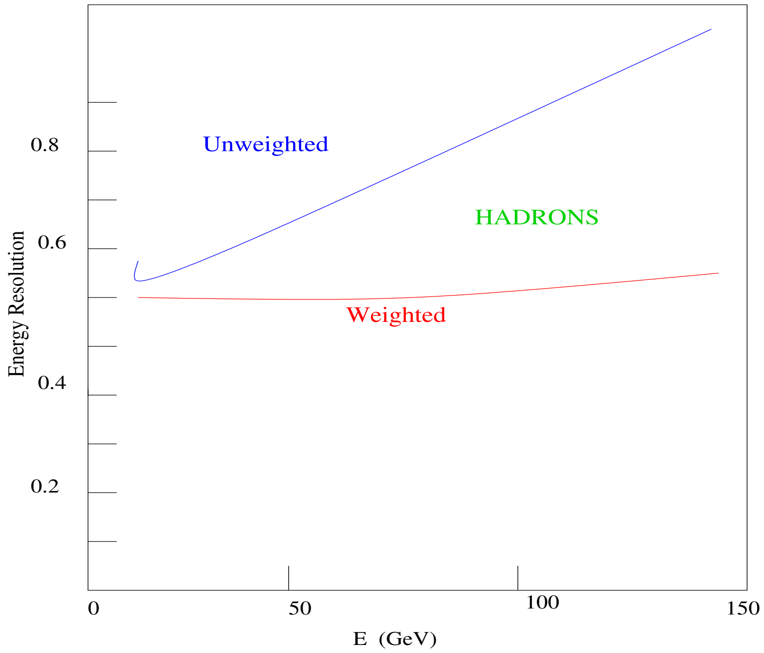

Figure 3.8: Energy resolution measured in the CDHS neutrino calorimeter versus the energy of the incident particle. With a weighting procedure to reduce the large fluctuation due to the electromagnetic component the resolution is improved, and is consistent with the $1/\sqrt{E}$ behaviour up to the highest energies measured [9].

3.2.3 Instrumental effects on the Energy resolution

Most hadronic calorimeters are *sampling* detectors, mainly using rather dense passive absorbers to reduce the linear dimensions of the instrument. Therefore, sampling fluctuations of statistical origin analogous to the case of electromagnetic ones should contribute to the energy resolution, although, for the sampling of the HC we do not have a similar and simple detailed description. Available measurements are consistent with a parametrization of the form:

$$\sigma(E)/E/hadron - sampling \cong 0.09\ [\Delta E\ (MeV)/E\ (GeV)]^{1/2}. \tag{3.19}$$

The quantity ΔE expresses the energy loss per unit sampling cell for minimum ionizing particles.

Energy leakage due to partial shower containment will not only degrade the energy resolution, but will also give rise to very asymmetric resolution functions with low-energy tails. Longitudinal fluctuations are larger than transverse fluctuations and hence longitudinal leakage is more critical to the performance.

3.2.4 Differences between the hadronic and electromagnetic showers

The dimensions and scale properties of both shower types are quite different:

- $\lambda_{inte} \sim A^{1/3}$.
- $X_0 \sim A/Z^2$.

The separation and identification of e, γ, π^0 versus hadrons works very well for a material of elevated Z in which the relation λ_{int}/X_0 reaches values of the order of 30.

The *invisible* energy generates peculiarities in the Hadronic Calorimeters. This energy comes from muons and neutrinos escaping out of the detector and the fraction of the incident energy devoted to break the targets with no *visible* mechanism. Several studies reveal that the *invisible* energy can reach the 40 % of the non-electromagnetic energy.

The range of signals to detect in a channel of a Hadronic Calorimeter is wider than in an electromagnetic calorimeter and in addition there appear strongly ionizing particles. Consequently they can show effects of saturation or effects of recombination. Therefore it appears a suppression of the detector signal, until a factor 5, with effects on the linearity (the calorimeter gives nonlinear response).

A crucial difference between the electromagnetic and hadronic showers is that in the last ones the neutrons (of several MeV) transport a considerable fraction of the incident energy, coming from the nuclear evaporation.

3.3 Effects of the e/h ratio on the calorimeter performance

We define as e the calorimeter response to the energy deposited through a purely electromagnetic process and h the response to the purely hadronic process, that means the response to a hadron substracted the electromagnetic part.

The ratio e/h is the relation between both responses. This ratio should be equal to 1.0 for optimal performace [10].

The sampling fluctuations and the fluctuations in the fraction of the energy deposited in the form of ionizing particles, mentioned before, have consequences for calorimetric hadron detection. Firstly, the signal distribution for hadrons of energy E will be broader than for electromagnetic showers at the same energy. Secondly, the average response (signal per unit of energy) will have a different value for electromagnetic and hadronic showers ($e/h \neq 1$). The latter will in general be smaller ($e/h > 1$).

In the development of a shower generated by a high-energy hadron some fraction (f_{em}) of the energy is usually spent on the production of π^0's and ν's. A hadron shower, therefore, has in general an electromagnetic (em) and a non-electromagnetic component (see figure 3.7). The fact that the ratio $e/h \neq 1$ has the following consequences for the calorimeter performance:

- The fluctuations in f_{em} give an additional contribution to the energy resolution.

- Because of the non-Gaussian nature of the fluctuations in f_{em} the energy resolution σ/E will not improve as $E^{-1/2}$ with increasing energy.

- The calorimeter signal is not proportional to the hadron energy (alinearity).

- The measured e/h ratio is energy dependent.

All these effects have been experimentally observed. This is ilustrated in figure 3.9, which shows experimental data on calorimetric hadron detection with and iron/plastic-scintillator ($e/h = 1.4$) calorimeter [14], and with uranium/plastic-scintillator [1] ($e/h = 1$). The calorimeter response for iron rises with energy, and consequently the e/h signal ratio decreases as the energy increases. This effect is absent for uranium, once the right ratio between active and passive layers has been chosen.

To avoid the confusion caused by the latter effect, we prefer to use the energy-independent quantity e/h^{intr}, which is an intrisic characteristic of a non-compensated calorimeter, given by the ratio of the mean values of the two curves in figure 3.7. The relation between the e/h^{intr} and e/h ratios is given by:

$$e/h\ (E) = \frac{e/h^{intr}}{1 - \langle f_{em}(E)\rangle[1 - e/h^{intr}]} \tag{3.20}$$

where

$$\langle f_{em}(E)\rangle = 0.1\ ln\ E\ (GeV) \tag{3.21}$$

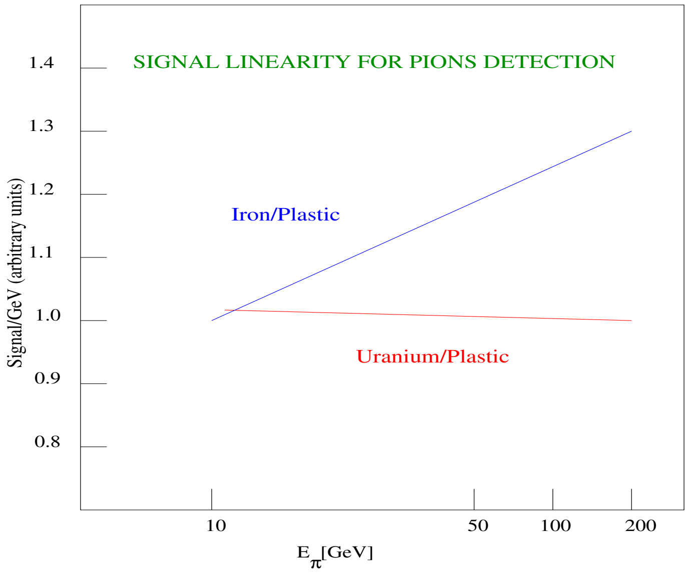

Figure 3.9: Linearity as a function of the energy from experimental data obtained with an iron/plastic-scintillator calorimeter, and with uranium/plastic-scintillator.

The figure 3.10 shows in a very clear way that, in particular at high energies, the value of e/h^{intr} is crucial for the energy resolution that can be obtained. For calorimeters with $e/h = 1.36$ at 10 GeV, the resolution σ/E does not become better than $\sim 7\%$, even at the highest energies. For calorimeters with $e/h^{intr} = 1$, the energy resolution will continue to improve with increasing energy, until limitations due to instrumental effects become important.

3.3.1 The e/h signal ratio

The e/h ratio depends on a large number of factors, of which we can emphasize:

- The Z of the active and passive media.
- The hydrogen content of the active medium.
- The saturation properties of the active medium.
- The nuclear level structure of the absorber.
- The size of the detector.
- The cross section for thermal neutron capture in the absorber.

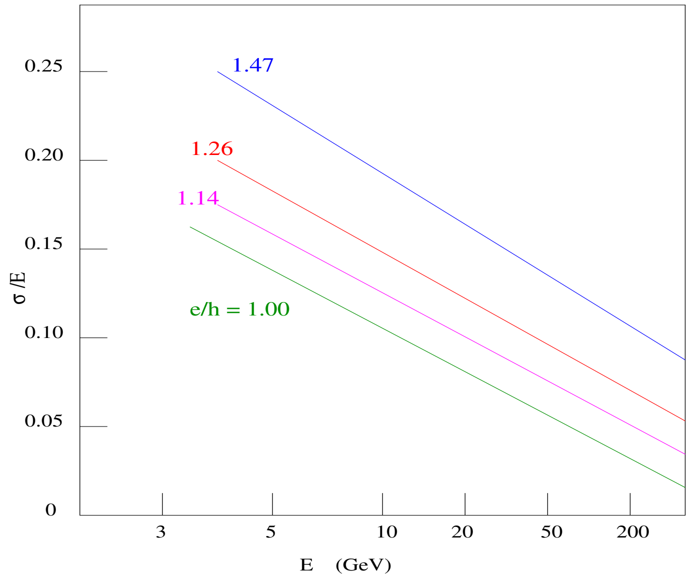

Figure 3.10: Monte Carlo simulation of the $e/h \neq 1$ effects on the energy resolution for hadron calorimeters.

- The signal integration time.
- The thickness of the active and passive layers.
- The sampling fraction.

The e/h ratio can therefore be tuned through the sampling fraction, and for the hydrogenous material (various plastic scintillators, TMP) an ideal sampling fraction ($e/h = 1$) exists.

The sensitivy of the e/h ratio with the sampling fraction depends on two factors:

- The fraction of hydrogen atoms in the active medium.
- The saturation of the active medium. Less saturation causes a larger sensitivity and consequentely leads to a larger optimal sampling fraction.

For calorimeters with nonhydrogenous active layers (e.g. LAr, Si), the effect of the sampling fraction on the relative contribution of neutrons to the calorimeter signal is absent. It turned out that the e/h ratio depends quite sensitively on the contribution of captured neutrons to the hadronic calorimeter signal, which can be tuned through the signal integration time.

In the nonelectromagnetic shower part inevitable losses that cannot be compensated will occur, e.g., the binding energy required to release protons or nucleons aggregates from their nuclear environment. Therefore, the e/h^{intr} signal ratio has always to be larger than 1.0 for such devices.

3.4 The Hadronic Tile Calorimeter of ATLAS

The Tile Calorimeter is one of the ATLAS sub-detectors. ATLAS is one of the general purpose pp detectors designed for the Large Hadron Collider (LHC) to be built at CERN. It is a large hadronic sampling calorimeter which makes use of iron as the absorber material and scintillating plates, read out by wavelength shifting (WLS) fibres, as the active medium. The new feature of its desing is the orientation of the scintillating tiles which are placed in planes perpendicular to the colliding beams and are staggered in depth. A good sampling homogeneity is obtained when the calorimeter is placed behind an electromagnetic compartment and a magnetic coil equivalent to a total of about two interaction lengths (λ) of material. This has been verified with Monte Carlo simulation and has been proved by the test beam results [13].

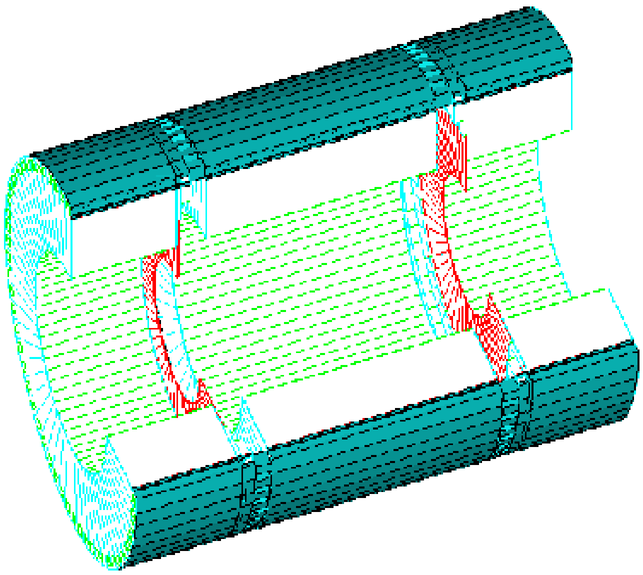

Figure 3.11: Layout view of the Tile Calorimeter barrel and extended barrels.

The Tile Calorimeter consist of a cylindrical structure with an inner radius of 2280 mm and an outer radius of 4230 mm. It is subdivided into a 5640 mm long central barrel and two 2910 mm extended barrels as shown in figure 3.11. The scintillating tiles lie in the $r - \phi$ plane and span the width of the module in the ϕ direction. WLS fibres running radially collect the light from the tiles along their two open edges. Readout cells are then defined by grouping together a set of fibres into a photomultipler (PMT), to obtain a three dimensional segmentation. Radially, the calorimeter is segmented into three layers, approximately 1.4, 3.9 and 1.8 interaction lengths thick at $\eta = 0$; the $\Delta\eta \times \Delta\phi$ segmentation is 0.1×0.1 (0.2×0.1 in the last radial layer). This calorimeter layout has been successfully proved with large-sized prototypes in the test beam area as a part of the RD34 project [14].

At the LHC, calorimeters will be the leading detectors in many measurements for the reconstruction of prime interest physics channels. In the region between the sensitivity limit of LEP2 ($\sim$ 98 GeV) and $m_H = 130$ GeV, the Higgs would most likely be observed in the $H \to \gamma\gamma$ channel, which will be reconstructed in the electromagnetic (EM) calorimeter. In the region $130 < m_H < 600$ GeV, the cleanest decay mode would be $H \to ZZ \to 4l$, and the reconstruction of final states containing two or four electrons will be mainly based on the EM calorimeter information. In the region $m_H > 600$ GeV, two decay channels are expected to be observable above the background: $H \to ZZ \to ll\nu\nu$, which requires excellent measurement of the missing transverse energy (E_T^{miss}) in the calorimeters to reduce the potentially large instrumental background, and $H \to WW \to l\ \nu\ jet\ jet$, which can only be detected above the background if the $W \to jet\ jet$ invariant mass can be accurately reconstructed in the calorimeters and the two forward jets, produced in association with the Higgs, can be tagged efficiently in the forward calorimeters.

3.4.1 The principle of the Detector

The tiles are placed radially and staggered in depth. The structure is periodic in z. The tiles are 3 mm thick and the total thickness of the iron plates in one period is 14 mm. The highly periodic structure of the system allows the construction of a large detector by assembling smaller sub-modules together. Since the mechanical assembly is completely independent from the optical instrumentation, the design becomes simple and cost effective. Simplicity has been the guideline for the light collection scheme: fibres are coupled radially to the tiles along the outside faces of each module; the laminated structure of the absorber allows the coupling of the fibres. The use of fibre read-out allows to define a logical cell structure, creating a projective geometry for triggering and energy reconstruction (see figure 3.12). A compact electronics system is housed in the girder of each module. Finally, the read-out of the two sides of each of the scintillating tiles into two separate photon detectors (in our case photomultipliers, PMTs) guarantees a sufficient light yield and provides a redundancy which might be needed during the long expected period of operation of the ATLAS experiment.

The Tile Calorimeter is designed as one barrel and two extended barrel hadron

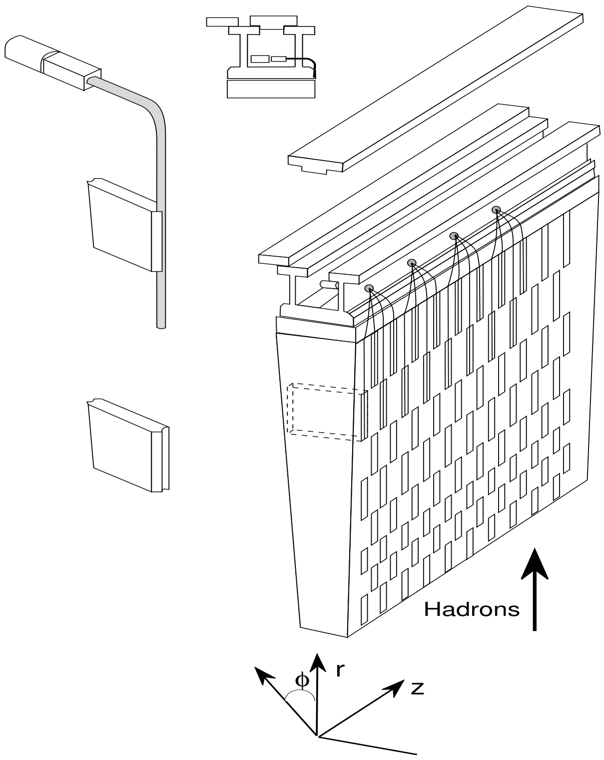

Figure 3.12: The principle of the Tile Calorimeter design.

parts with cylindrical structure. Each detector cylinder is built of 64 independent wedges along the azimuthal direction. Between the barrel and the extended barrels there is a gap of about 600 mm (see figure 3.13), which is needed for the Inner Detector and the Liquid Argon cables, electronics and services. The barrel covers the region $-1.0 < |\eta| < 1.0$, and the extended barrels cover the region $0.8 < |\eta| < 1.7$.

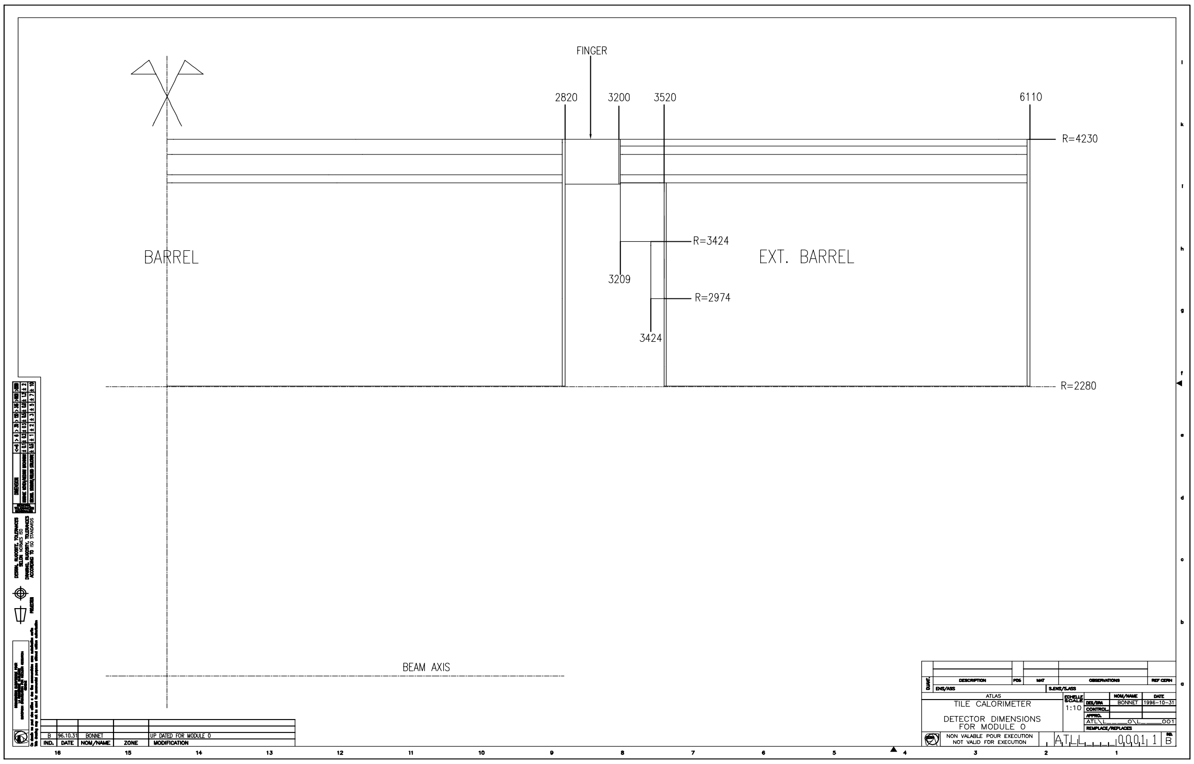

Figure 3.13: Overall schematic view of the Tile Calorimeter detector dimensions.

Part of the gap contains an extension of the extended barrel: the Intermediate Tile Calorimeter (ITC), which is a structure stepped in order to maximize the volume of the active material in this region, leaving still room for the services and cables. The ITC consists of a calorimeter pluged between the region $0.8 < |\eta| < 1.0$ and, due to severe space constraints, only scintillator between $1.0 < |\eta| < 1.6$. The scintillators in the region $1.0 < |\eta| < 1.2$ are called *gap scintillators*, and the scintillators between $1.2 < |\eta| < 1.6$ are called *crack scintillators*. These last ones extended down to the region in between the barrel and the end-cap cryostats. While the plug and the gap scintillators primarily provide hadronic shower sampling, the crack scintillator plays a critical role in sampling electromagnetic showers, where the normal sampling is comprised by the dead material of the cryostat walls and the inner detector cables.

The Tile Calorimeter forms the shell of the inner part of the ATLAS detector. Within its volume, once the barrel and the extended barrels are assembled, all the sub-detectors except the muon system will be placed. The massive iron structure is rigid enough to support their weight, with the most important components being the full Liquid Argon cryostat and the solenoid. The structure of the Tile Calorimeter as well as the corresponding to all the other sub-detectors inside it is self-supporting and has no mechanical connection with the outside muon system.

3.4.1.1 Detector environment: Radiation and Magnetic field

As mentioned above, the Tile Calorimeter sorrounds the Inner Detector and the Liquid Argon Calorimeter. Due to its position, the detector has to face three basic problems which have implications for its final performance: the level of radiation, the presence of the two magnetic fields from the inner solenoid and the outer toroids, and finally the amount and the $|\eta|$ distribution of the dead material in front of the calorimeter itself.

The dominant source of radiation in the ATLAS detector comes from the pp interaction rate, which is of the order of 10^9 interactions per second and per collision point. Other sources of radiation such as beam losses or beam gas interactions are expected to be at least two orders of magnitude smaller.

When the high energy particles produced at the interaction point enter in the detector material, they begin to develop the shower. If the material is thick (as is the case of a calorimeter) the shower will develop until most of the charged particles are absorbed and only neutrons and associated photons remain and most likely escape from the calorimeter volume. In figure 3.14 the isodose map of the inner detector and the calorimeters is shown. For most of the Tile Calorimeter volume the annual dose rates are below the 20 $Gy\ yr^{-1}$ line, with a maximum annual dose expected of $\sim 36\ Gy$, at $\eta = 1.2$. These radiation levels can affect the performance of the calorimeter over the long period of running due to the degradation in the light production and/or transmission in the scintillators and fibres.

A large program of irradiation test has been performed for the active components of the detector. Different tile/fibre setups have been irradiated with doses from 650 *Gy* to 10 *kGy*, at rates from 15 *kGy/h* down to 5.5 Gy/h. For 10 years of high luminosity running at LHC, a light loss of no more than 5% is expected in the tiles of the first longitudinal sampling, and even less for the others. Using those results and assuming no radiation damage for the Liquid Argon Calorimeter, the energy resolution and jet signal degradation is negligible.

The Tile Calorimeter is the return path for the flux of the solenoid, 70% of which passes through the girder structure, 25% through the active parts of the calorimeter return, and about 2% through the front-plates. A 3D simulation program has been

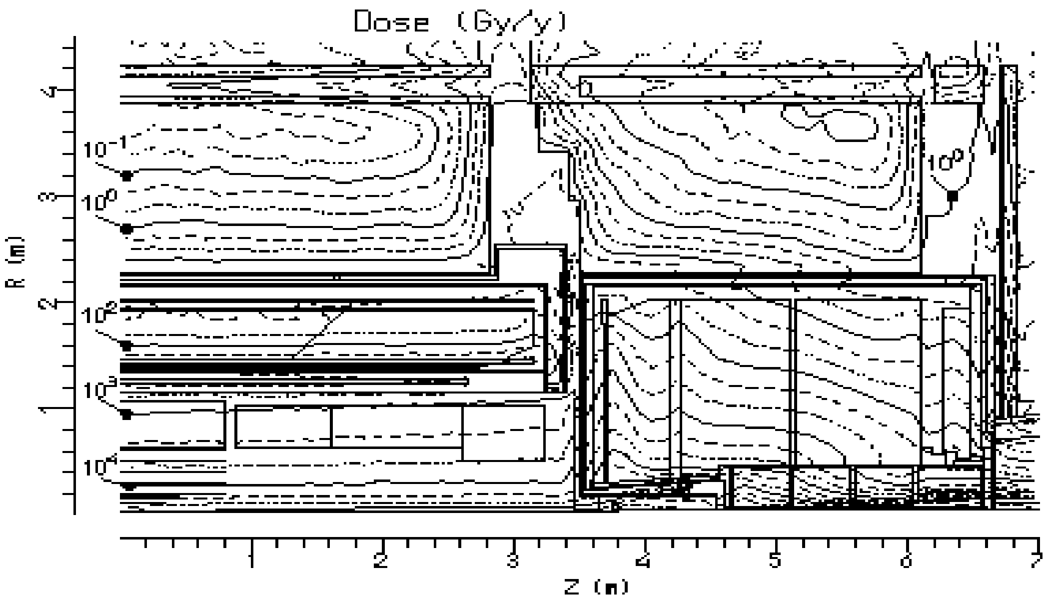

Figure 3.14: Yearly integrated dose ($Gy\, yr^{-1}$) in the inner detector and the calorimeters.

used to calculate the magnetic field at each point of the detector [15]. The highest field regions are at the outer edges of the barrel and extended barrels, with the maximum value, due to the toroid stray field of ~ 1.5 T, located at the outer girder radius. The maximum value in the scintillator does not exceed 6 ± 2 mT. Inside the girder region, the maximum varies from 80 mT at $R = 38$ m to 200 mT at $R = 4.2$ m. The influence of the magentic field on the scintillator light yield has been studied: the light output will increase by about $\sim 1\%$ as a consequence of the expected magnetic field. This value is well within the accuracy of the cell-to-cell intercalibration.

3.4.2 Physics requirements

The tasks of the calorimeters at hadron colliders are:

- accurate measurement of the energy and position of electrons and photons;

- measurement of the energy and direction of jets, and of the missing transverse momentum of the event;

- particle identification, for instance separation of electrons and photons from hadrons and jets, and of τ hadronic decays from jets;

• event selection at the trigger level.

The Standard Model (SM, [16]) Higgs search imposes specific requirements to the hadronic calorimetry. The $W \to jet - jet$ mass reconstruction and the forward jet tagging are crucial for discovering a high mass Higgs boson, and the $H \to b\bar{b}$ mass reconstruction using jet spectroscopy is important for the low mass Higgs search. Both jet identification and jet spectroscopy are clearly mandatory for studying top physics. In the Minimal Supersymmetric Standard Model (MSSM, [17]) a large region of the parameter space is covered by the detection of A^0/H^0 decays into $\tau\tau$ pairs; the $\tau\tau$ mass reconstruction is critically dependent of good p_T^{miss} resolution. In supersymmetric (SUSY, [18]) models, the need to detect the presence of non-interacting particles sets stringent limits on the hermeticity of the calorimeters. The study of quark compositness requires good measurement of very high-p_T jets and good linearity of response, as its effects would be observable as deviation from the QCD expectations in the high-p_T region of the jet cross-section. This set of examples, together with the SM Higgs is used for illustrating the physics requirements on hadronic calorimetry both in the inital low-luminosity phase and in the subsequent high-luminosity running, but it is by no means complete of all the physical issues that will be covered by ATLAS.

The ambitious physics programme of the LHC and the difficult experimental environment set stringent and challenging requirements on the detector specifications; all these will be discussed in the next section.

3.4.2.1 Hadronic calorimeter requirements

The general features of the hadronic calorimetry in terms of rapidity coverage, granularity, energy resolution, energy linearity, total thickness, noise, time of response, are:

• Rapidity Coverage: The main calorimeter task is the reconstruction of jets and the measurement of the event p_T missing. The jet detection has to extend to $|\eta| = 5$ for allowing an efficient tagging of the forward jets associated to the production of heavy Higgs, and the same η coverage is needed for a good missing p_T resolution.

• Granularity: The most stringent transverse granularity requirement comes from the $W \to jet - jet$ decay at high-p_T and applies for $|\eta| < 3$, where a granularity $\Delta\eta \times \Delta\phi = 0.1 \times 0.1$ is needed.

• Energy resolution: For the hadronic calorimeter the guidelines for the energy resolution performances are set requiring a jet energy resolution at different levels in different η regions

$$\frac{\sigma}{E} = \frac{\mathbf{50\%}}{\sqrt{E}} \oplus \mathbf{3\%} \tag{3.22}$$

for $|\eta| < 3$ and

$$\frac{\sigma}{E} = \frac{\mathbf{100\%}}{\sqrt{E}} \oplus \mathbf{10\%} \tag{3.23}$$

for $3 < |\eta| < 5$

Such resolutions are adequate to the tasks of providing jet reconstruction and jet-jet mass reconstruction as well as missing p_T measurement for physical processes of interest.

• Energy linearity: The most stringent linearity requirements for the hadronic calorimeter come from the study of quark compositness, where the jet energy scale has to be linear within 2% up to a transverse energy of 4 TeV [19].

• Total thickness: A total calorimeter (EM and hadronic) thickness of about 10 interaction lengths (λ) is required for shower containment, both for energy resolution reasons and for reducing the background in the muon chambers.

• Noise: The electronic noise level in the hadronic calorimeter is relevant at low luminosity for the quality of low energy jet reconstruction, but for this, as well as for the missing E_T reconstruction the dominant effects come from the EM calorimeter due to its high number of channels.

• Speed of response: A signal peaking time of $\sim$ 40 nanoseconds is required for minimizing the total noise (electronic and pile-up) at high luminosity.

A hadronic calorimeter with the above features is adequate for coping with the physics requirements listed in Section 3.4.2, because it is thus able to perform the critical tasks required. A short list of these tasks is given here:

• Jet identification and measurement: The jet performances are given as a function of η, taking into account the effects intrisically related to the quality of the calorimetry and the ones that would exist even with a perfect calorimeter, due to the energy carried away by neutrinos and muons or lost outside of the angular region used for the jet reconstruction and to pile-up.

The accuracy of the absolute jet calibration scale is a stringent requirement, e.g. for a precise measurement of the top quark mass and for the search of compositness.

• Jet-jet mass reconstruction: At low luminosity the aim is to approach a 1% error on the top quark mass reconstruction. At high luminosity the goal is the detection of a heavy SM Higgs boson decaying into a high-p_T $W \rightarrow jet - jet$, where the jet-jet mass reconstruction is the crucial point.

• Forward jet tagging: The acceptance region for the high-mass Higgs search with forward jet tagging is $2 < \eta < 5$. A smooth transition (at $\eta \sim 3.1$) to the forward-calorimetry region and a good performance of the forward calorimeter are key issues in this domain.

• E_T^{miss} reconstruction: The E_T^{miss} plays an essential role from two different points of view. First, the achievement of a good resolution is mandatory for the $\tau\tau$ mass reconstruction, and second, a very good control of the tails of the E_T^{miss} distribution is required for keeping low the level of the fake E_T^{miss} background. This background affects the search for SUSY particles, coming mainly from multijet events, and the search for $H \rightarrow ZZ \rightarrow ll\nu\nu$, coming mainly from Z+jets events. For the control of E_T^{miss} tails the critical regions are of course the cracks in the calorimeters.

All the requirements mentioned above can be summarized in table 3.2.

Table 3.2: *Physical hadronic calorimeter requirements.*

Hadronic calorimeter performances	
Rapidity Coverage	$\|\eta\| < \sim 5$
Granularity	$\Delta\eta \times \Delta\phi = 0.1 \times 0.1$ for $\|\eta\| \leq 3$
	$\Delta\eta \times \Delta\phi = 0.2 \times 0.2$ for $\|\eta\| > 3$
Energy resolution	$\frac{50\%}{\sqrt{E}} \oplus 3\%$ for $\|\eta\| \leq 3$
	$\frac{100\%}{\sqrt{E}} \oplus 10\%$ for $3 < \|\eta\| < 5$
Energy linearity	2 % up to a transverse energy of 4 TeV
Total thickness	10 interaction lengths (λ)
Noise	less than the 5 GeV (low energy jet)
Speed of response	40 nanoseconds
Jet identification	1% accuracy
Jet-jet mass reconstruction	1 % error on the top mass
Forward jet tagging	acceptance region $2 < \|\eta\| < 5$
$E_T^{miss} reconstruction$	good resolution for the $\tau\tau$ mass

Bibliography

[1] H. Messel and D. F. Crawfird, Electron-photon shower distribution: Function tables for lead, copper and air absorbers, Pergamon Press, London (1970).

[2] Y. S. Tsai, Rev. Mod. Phys. 46:815 (1974).

[3] E. Longo and I. Sestili, Nucl. Instrum. Methods 128:283 (1975).

[4] A. N. Diddens et al., Nucl. Instrum. Methods 178:27 (1980).

[5] U. Amaldi, Phys. Scripta 23:409 (1981).

[6] J. Ranft, Particle Accelerators 3:129 (1972); A. Baroncelli, Nucl. Instrum. Methods 118:445 (1974); T. A. Gabriel et al., Nucl. Instrum. Methods 134:271 (1976).

[7] Amendikua, S. R. et al., report Pisa 80-4 (29 May 1980), Contribution to the Conference on Experimentation at LEP, Uppsala, June 1980.

[8] W. Hofmann et al., Nucl. Instr. and Methods 163, 77 (1979).

[9] E. Gabathuler et al., Nucl. Instr. and Methods 120, 391 (1974).

[10] C. W. Fabjan and W. J. Willis, in: Proc. Calorimeter Workshop, ed., M. Atac, Batavia Illinois (1975) p. l.

[11] H. Abramowicz et al., Nulc. Instr. and Meth. 180 (1981) 429.

[12] T. Akesson et al., Performance of the Uranium/Plastic Scintilator Calorimeter for the HELIOS Experiment at CERN, CERN-EP/87-111.

[13] ATLAS Tile Calorimeter Technical Design Report, CERN/LHCC/96-42 (1996).

[14] E. Berger et al., (RD34 Collaboration), Construction and Performance of an Iron-scintillator Hadron Calorimeter with Longitudinal Tile Calorimeter Configuration. CERN/LHCC 95-44,CERN, Geneva, Switzerland.

[15] Preliminary results on the ATLAS solenoid magnetic field calculations in presence of hadronic tile calorimeter. V. Klyuklin and B. Klochkov, 31-01-1994; Calculation of the ATLAS magnetic field. F. Bergsma, 16-08-1995.

[16] S.L. Glashow, Nucl. Phys. 22, 579 (1961). S. Weinberg, Phys. Rev. Lett. 19, 1264 (1967). A. Salma, Elementary Particle Theory, H. Svartholm, ed. (Stockholm: Almquist and Wiksell, 1986).

[17] Z. Kunszt and F. Zwirner, Nucl. Phys. B385, 3 (1992).

[18] S. P. Martin, A Supersymmetry Primer, hep-ph/9709356.

[19] ATLAS Collaboration, Technical Proposal, CERN/LHCC/94-43, LHCC/P2.